2022-01-0917 Published 29 Mar 2022

Dynamic Formulation of the Utility Truck with the Morphing Boom Equipment

Parth Y. Patel and Vladimir Vantsevich University of Alabama at Birmingham

Gemunu Happawana California State University

Chris Harned and David Boger Altec Inc.

Citation: Patel, P.Y., Vantsevich, V., Happawana, G., Harned, C. et al., "Dynamic Formulation of the Utility Truck with the Morphing Boom Equipment," SAE Technical Paper 2022-01-0917, 2022, doi:10.4271/2022-01-0917.

Received: 22 Jan 2022 Revised: 22 Jan 2022 Accepted: 12 Jan 2022

Abstract

Robotic technology has begun to play an essential role in ground automotive applications. Utility trucks are among the first responders in extreme climate and severe weather conditions, comprised of two systems: a mobile platform and an articulated robotic morphing arm. The conventional industrial manipulators are mounted on stationary bases, while a mobile manipulator is dynamically coupled on a mobile platform. Such trucks with morphing manipulator can increase the possibility of road accidents in many ways and, additionally, create dangerous situations on the roads, and off-road conditions, while moving, and performing tasks. Large boom equipped trucks for reaching elevated heights can become unstable due to drastic variation of the boom equipment moment of inertia causing the extreme weight re-distribution among the wheels. The morphing capabilities of the utility trucks need to be investigated together with the vehicle-road forces in order to hold the truck safe on the roads. In this paper, a novel method and mathematical models are represented to investigate the morphing dynamics of a multi-body combination of the boom equipment manipulator, and the utility truck. This approach integrates the morphing dynamics of the boom equipment with the conventional dynamics of the utility truck and, thus, to manage the dynamic normal reactions of four wheels. The mathematical model of the multi-body combination of the boom equipment are presented and implemented symbolically in compact form with the use of the recursive Newton-Euler dynamic formulation. The multibody 7 degree-of-freedom dynamics of the utility truck with the sprung and unsprung masses is conventional and thus, only dynamics of the boom equipment is included in this paper.

Keywords

Utility truck; Morphing Boom Equipment; Dynamic Analysis; Recursive Newton-Euler Method.

Introduction

Industrial robots do not look like humans, but they can perform several undesirable tasks for humans. All the industrial robots are mechanical handling devices which a computer control can manipulate. The manipulator or the automated handling device outdoes the arm of a human. All the manipulator joints are driven by pneumatic, hydraulic, or electric actuators which gives more potential power than human beings. At present, more researchers are focusing on mobile manipulators that are dynamically coupled with the mobile platform/vehicle in dangerous and hazardous environments to perform undesirable tasks [1-6].

Manipulators were used either for industrial or research purposes during the early stages of robotics. Manipulators have been employed in different sectors like military, marine, construction, forestry, space agriculture, mining, and nuclear [7]. These manipulators are generally mobile and mounted on a moving base. The field manipulators are very beneficial in mining because they are remotely operated, and autonomous technology could eventually eliminate the need for the miners to travel intensely underground [8]. However, heavy-duty work has many difficulties, i.e., applications in Civil Engineering (building maintenance, concrete pouring, saving people's lives, etc.). A large manipulator with sufficient power is required [9]. One of the severe problems is that the base is not fixed, and thus, the compliance due to the vehicle tires and suspension affects the manipulator accuracy. The various problems include modeling and control systems, mobility, hardware weight and stability, sensing, and environmental factor [10].

According to the US Census Bureau, there are approximately 15 million trucks currently in operation across the

country operated by 2.83 million drivers, 28.2% of whom drive various utility trucks [11]. Utility trucks (also known as boom trucks) are the first responders in extreme climate and weather situations for cutting trees to restore traffic, for recovering living beings from destroyed properties, for repairing electric posts and restoring power. Such trucks with morphing capabilities of the manipulator can increase the possibility of road accidents in several ways and, furthermore, create hazardous situations on the roads, and off-road conditions while moving and performing tasks. Large bucket/boom trucks for reaching elevated heights can become unstable due to their geometry change, which can cause a drastic variation of the truck-boom system's moment of inertia, and the extreme weight re-distribution between the wheels. Multiplied by the design instability of the utility trucks, such conditions may have a serious impact on the truck's safety. By determining the smart morphological properties of the entire utility truck's 3D perimeter, it is possible to achieve a better distribution of the normal load on the wheels and, thus, to provide more tire grip/traction.

In this analysis, the boom equipment, which morphs its geometry and orientation relative to the utility truck frame, is considered as a 5 degree-of-freedom (DOF) robotic manipulator. The morphing dynamics of the boom equipment majorly impact the wheel dynamic normal reactions. Such agile managing of the wheel dynamic normal reactions is a crucial component of the Aerodynamic Intelligent Morphing System (A-IMS) that should stabilize the motion of the autonomous smart utility truck under hazardous environmental conditions. Therefore, the dynamics of the boom equipment must need to be investigated along with the conventional 7-DOF dynamics of the utility truck with the sprung and unsprung masses.

This paper reports a developed mathematical dynamic model and a simple PD control for the boom equipment, and a novel approach, a method to integrate the morphing dynamics of the boom equipment with the conventional dynamics of the utility truck. A recursive Newton-Euler method is implemented symbolically in compact form to analyze the dynamics of the boom equipment. Parameters for the developed dynamical model of the boom equipment were obtained from actual measurements, drawings, and solid modelling techniques. Finally, the paper concludes with the simulation results of the boom equipment system and its response when morphing from one position to the designated location. In this study, F450 utility truck with the morphing boom equipment attached to it was used for the analysis.

Overview of the Utility Truck

Utility trucks are heavy-duty mobile systems capable of working in extreme conditions. The boom equipment is considered as a 5 degree-of-freedom (DOF) articulated manipulator in this research, and kinematic and dynamic modeling methodologies which are routinely applied in robotics are applied to the boom equipment. The utility truck with the boom equipment is shown in Figures 1 and 2.

FIGURE 1 Configuration and component identification of the utility truck.

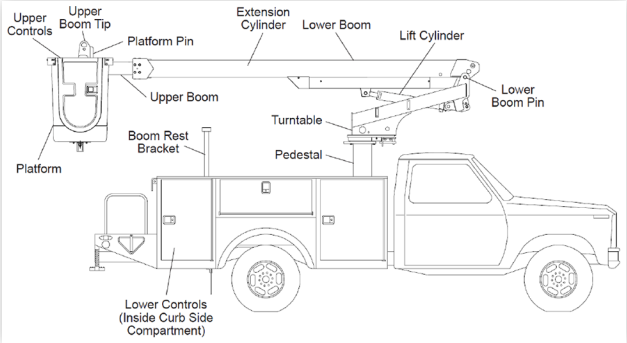

FIGURE 2 2D Drawing of a utility truck on horizontal surface.

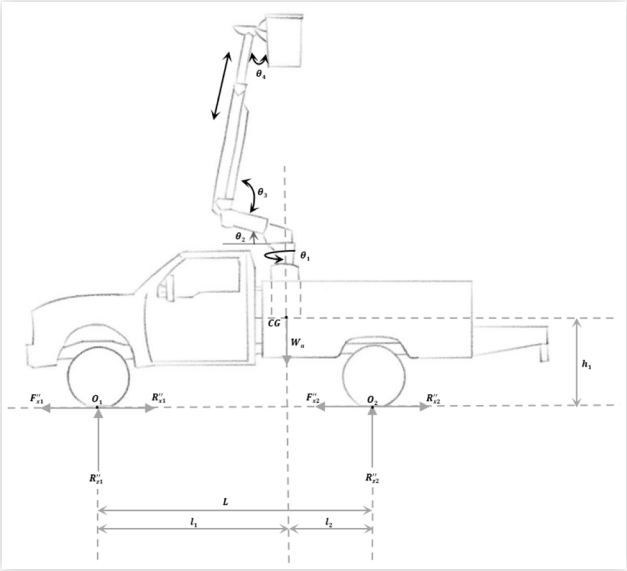

TABLE 1 Constrained of utility truck's boom geometry

Parameter	Working Range
Turntable Angle (θ_1)	-15.0 to 370 degrees
Turntable Boom Angle (θ_2)	15 degrees
Boom Articulation Angle (θ_3)	-13.5 to 80 degrees
Bucket Articulation Angle (θ_4)	0 to 76 degrees
Upper Boom	3.863 meters

Figure 1 represents the configuration and component identification of the utility truck, while Figure 2 represents a two-dimensional drawing of the utility truck's mass and geometry on a horizontal surface.

The constraint imposed by the truck's boom geometry [12] are listed in Table 1.

Dynamic Modeling

It is essential to obtain dynamics of the system to improve performance, design, simulate the behavior, and finally

FIGURE 3 Link frame attachment to the 5 dof system.

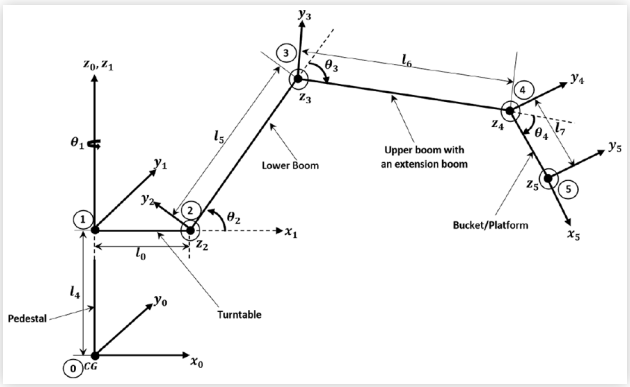

TABLE 2 D-H parameters for the 5 dof system

i	α_{i-1}	a_{i-1}	d_i	θ_i
1	0	0	l_4	θ_1
2	$\frac{\pi}{2}$	l_0	0	θ_2
3	0	l_5	0	θ_3
4	0	l_6	0	θ_4
5	0	l_7	0	-

control a system. But, first, a kinematic model is required to develop the dynamics of the boom equipment. The kinematics modeling is done first by attaching frames to the joint of every link to get the rotation matrices. The usual convention to attach frames to every link of a manipulator is called Denavit-Hartenberg (D-H) notation [13]. However, a non-standard D-H method is utilized in this paper as described by Craig [14]. An advantage of using the non-standard D-H method over the standard D-H method is that the rotation θ_i is around z_i-axis and the joint number is the same as the coordinate number. The actuation force, which is exerted at joint i, is also at the same place as the defined coordinate frame at that joint. Additionally, addressing the link's geometrical characteristics, such as the center of gravity, are more natural in this system. According to the non-standard D-H notation, the boom equipment is described kinematically by four parameters for each link, and the link frames are attached as described by Craig [14]. The link frames used for the pedestal, turntable, lower boom, upper boom with an extension boom, and a bucket are shown in Figure 3. Here, the boom equipment is considered as a 5-DOF manipulator which has four revolute joints i.e., θ_1 to θ_4 and one prismatic joint between upper boom and an extension boom.

The fixed frame is represented by $x_0y_0z_0$ axes. The corresponding table of D-H parameter is shown in Table 2. Lengths, l_0, l_5, l_6 and l_7 are the turntable, lower boom, upper boom with an extension and bucket lengths respectively. The distance from the fixed frame to turntable frame along z_0 axis is denoted by l_4 and θ_i is the joint variable of ith joint.

The general form of the transformation matrices can be obtained by the following formula provided in [14].

$$ {}^{i-1}T_i = \begin{bmatrix} \cos\theta_i & -\sin\theta_i & 0 & a_{i-1} \\ \sin\theta_i\cos\alpha_{i-1} & \cos\theta_i\cos\alpha_{i-1} & -\sin\alpha_{i-1} & -\sin\alpha_{i-1}d_i \\ \sin\theta_i\sin\alpha_{i-1} & \cos\theta_i\sin\alpha_{i-1} & \cos\alpha_{i-1} & \cos\alpha_{i-1}d_i \\ 0 & 0 & 0 & 1 \end{bmatrix} \quad (1) $$

Using Eq. (1) and Table 2, the transformation matrices from the fixed frame to turntable, turntable to lower boom, lower boom to upper boom and upper boom to bucket are found as below

$$ {}^{0}T_1 = \begin{bmatrix} \cos\theta_1 & -\sin\theta_1 & 0 & 0 \\ \sin\theta_1 & \cos\theta_1 & 0 & 0 \\ 0 & 0 & 1 & l_4 \\ 0 & 0 & 0 & 1 \end{bmatrix} {}^{1}T_2 = \begin{bmatrix} \cos\theta_2 & -\sin\theta_2 & 0 & l_0 \\ 0 & 0 & -1 & 0 \\ \sin\theta_2 & \cos\theta_2 & 0 & 0 \\ 0 & 0 & 0 & 1 \end{bmatrix} $$

$$ {}^{2}T_3 = \begin{bmatrix} \cos\theta_3 & -\sin\theta_3 & 0 & l_5 \\ \sin\theta_3 & \cos\theta_3 & 0 & 0 \\ 0 & 0 & 1 & 0 \\ 0 & 0 & 0 & 1 \end{bmatrix} {}^{3}T_4 = \begin{bmatrix} \cos\theta_4 & -\sin\theta_4 & 0 & l_6 \\ \sin\theta_4 & \cos\theta_4 & 0 & 0 \\ 0 & 0 & 1 & 0 \\ 0 & 0 & 0 & 1 \end{bmatrix} \quad (2) $$

$$ {}^{4}T_5 = \begin{bmatrix} 1 & 0 & 0 & l_7 \\ 0 & 1 & 0 & 0 \\ 0 & 0 & 1 & 0 \\ 0 & 0 & 0 & 1 \end{bmatrix} $$

The dynamics of the robot manipulators can be described mathematically in different ways, which explicitly describes the relationship between force and motion. These equations are required in the simulation of robot manipulator motion and the control algorithms. The boom equipment manipulator dynamics can be derived in various ways, namely using a recursive Newton-Euler dynamic formulation, Kane's method, a Lagrangian formulation, and others. In this study, the Newton-Euler dynamical formulation was used to derive the dynamic equations of the boom equipment. The Newton-Euler dynamical formulation is the preferred choice for a manipulator with more degrees of freedom because of its recursive structure, and it's easy to implement in the form of computer code and takes shorter computational time [15, 16]. Furthermore, the recursion will be significantly simplified when the frames are attached conveniently. In general, in recursive Newton-Euler method, kinematic quantities i.e., velocities and accelerations are computed starting from fixed base to the end tip of the bucket, while actuator forces and torques are calculated with inward computations.

The basis of Newton-Euler method is based on following three important laws:

- As Newton states in his second law that every action has an equal and opposite reaction. Thus, if link (i-1) applies force f and torque τ to the link i, then link i applies a force - f and torque -τ to link (i-1).
- The rate of change of the linear momentum of a link is equal to the total force applied to that link.

FIGURE 4 Forces and torques acting on link *i*

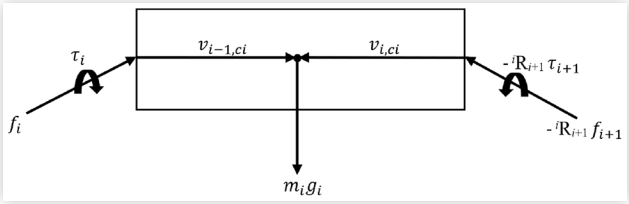

- The rate of change of angular momentum of a link is equal to the total torque applied to the link.

In conclusion, the Newton-Euler method can be summarized with the force balance and torque balance equations as

$$f = ma \tag{3}$$

$$\tau = \omega \times (I\omega) + I\dot{\omega} \tag{4}$$

where, m is the mass of the link, a is the acceleration of the center of mass, I is the inertia tensor of the link at the center of mass, ω is angular velocity of the link, and $\dot{\omega}$ is the angular acceleration of the link.

Equation of an N-Link Manipulator Figure 4 represents a link i together with all forces and torques acting on it. By the Newton's second law, f_i is the force applied by link (i-1) on link i, and $-f_{i+1}$ is the force applied by link (i+1) on link i. According to the definition described above, f_i is expressed in frame i while $-f_{i+1}$ is expressed in the frame (i+1). Hence, to express both forces in frame i, it is essential to multiply the rotation matrix with ${}^{i}R_{i+1}$. The same definition applies to the torque and thus, force and torque balance equation based on equation (3, 4) becomes

$$\sum_{link} f = ma \tag{5}$$

$$f_i = {}^{i}R_{i+1} f_{i+1} + m_i a_{c,i} - m_i g_i \tag{6}$$

$$\sum_{link} \tau = \omega \times (I\omega) + I\dot{\omega} \tag{7}$$

$$\tau_i = {}^{i}R_{i+1}\tau_{i+1} - v_{i-1,ci} + ({}^{i}R_{i+1} f_{i+1}) \times v_{i,ci} + \omega_i \times (I_i \omega_i) + I_i \dot{\omega}_i \tag{8}$$

where, $a_{c,i}$ = linear acceleration vector of the center of mass of link i.

$a_{e,i}$= linear acceleration vector of the end of link i in coordinate frame i.

ω_i= angular velocity vector of link i with respect to frame 0.

$\dot{\omega}_i$= angular acceleration vector of link i with respect to frame 0.

g_i= acceleration due to gravity.

m_i= mass of link i.

$I_i = \begin{bmatrix} I_{ixx} & 0 & 0 \\ 0 & I_{iyy} & 0 \\ 0 & 0 & I_{izz} \end{bmatrix}$, inertia tensor of link i with respect to the center of mass of link i expressed in a frame located at the center of mass of the link i.

$v_{i-1,ci}$ = position vector from the origin of frame (i-1) to the center of mass of link i.

$v_{i-1,i}$ = position vector from the origin of frame (i-1) to the origin of frame i.

$v_{i,ci}$ = position vector from the origin of frame i to the center of mass of link i

${}^{i}R_{i+1}$ = rotation matrix from frame i to frame (i+1)

z_i = rotation of joint i expressed in frame i

The force balance equation is a part of the moment balance equation. Solving equation (8) for decreasing i and substituting equation (6) is the ultimate goal of the Newton-Euler formulation, but the solution requires to be expressed only by $\theta, \dot{\theta}, \ddot{\theta}$, which means it is necessary to find a relation between $\theta, \dot{\theta}, \ddot{\theta}$, and $a_{c,i}, \omega_i, \dot{\omega}_i$. This can be achieve by a recursive procedure of increasing i using following equations

$$\omega_i = {}^{i}R_{i-1}\omega_{i-1} + z_i\dot{\theta}_i \tag{9}$$

$$\dot{\omega}_i = \frac{d}{dt}(\omega_i) \tag{10}$$

$$a_{e,i} = {}^{i}R_{i-1}a_{e,i-1} + \dot{\omega}_i \times v_{i-1,i} + \omega_i \times (\omega_i \times v_{i-1,i}) \tag{11}$$

$$a_{c,i} = {}^{i}R_{i-1}a_{c,i-1} + \dot{\omega}_i \times v_{i-1,ci} + \omega_i \times (\omega_i \times v_{i-1,ci}) \tag{12}$$

This completes the recursive Newton-Euler formulation of an n-link manipulator. A more detailed description of recursive Newton-Euler algorithm can be found in [14].

The Dynamic Model of the Boom Equipment

Following assumptions have been made in the formulation of the dynamics of the boom equipment.

- All joints in the boom equipment's kinematic chain are considered single-degree-of-freedom joints, such that the torque applied at the joints are scalars about the rotation axis. The other two components (generated because of the coupled kinematics of the system) of the torque do not induce motion of θ_i.
- The dynamics of the hydraulic actuators are not included. Instead, an assumption is made that the hydraulic actuators act as infinitely powerful force sources, in the same way as represented in [17, 18]. Thus, it formulates a conservative dynamic model (13), which does not consider of non-conservative forces such as viscous and static friction forces and the dynamic model can be written on matrix form as

$$M(\theta)\ddot{\theta} + C(\theta,\dot{\theta})\dot{\theta} + g(\theta) = \tau \tag{13}$$

- An assumption of a fixed based system is made i.e., the turntable is placed on a rigid platform and the initial conditions are given by,

$$\omega_0 = \dot{\omega}_0 = 0 \tag{14}$$

- The boom equipment is moving in a free space, so no external forces and torques are applied at the end of bucket i.e., $f_5 = \tau_5 = 0$.
- The mass distribution in all the links is assumed as a symmetric with respect to the attached frame. Thus, inertia tensor will be diagonal and cross product of inertia are considered as an identically zero. Also, inertia tensor of all links is calculated at the center of mass of the link according to the Newton-Euler formulation. Hence, parallel axis theorem is employed to calculate inertia tensor at the center of mass of the link.

The rotation matrices needed to derive the dynamic model of the boom equipment can be found from first three rows and columns of transformation matrices of Eq. (1).

$$
{}^{0}R_1 = \begin{bmatrix} \cos\theta_1 & -\sin\theta_1 & 0 \\ \sin\theta_1 & \cos\theta_1 & 0 \\ 0 & 0 & 1 \end{bmatrix}, {}^{1}R_2 = \begin{bmatrix} \cos\theta_2 & -\sin\theta_2 & 0 \\ 0 & 0 & -1 \\ \sin\theta_2 & \cos\theta_2 & 0 \end{bmatrix}
$$

$$
{}^{2}R_3 = \begin{bmatrix} \cos\theta_3 & -\sin\theta_3 & 0 \\ \sin\theta_3 & \cos\theta_3 & 0 \\ 0 & 0 & 1 \end{bmatrix}, {}^{3}R_4 = \begin{bmatrix} \cos\theta_4 & -\sin\theta_4 & 0 \\ \sin\theta_4 & \cos\theta_4 & 0 \\ 0 & 0 & 1 \end{bmatrix} \tag{15}
$$

Forward recursion for kinematics, starting from turntable to the bucket:

For turntable (link 1),

Angular velocity and acceleration vector are calculated using equation (9, 10) respectively,

$$\omega_1 = z_1\dot{\theta}_1 \tag{16}$$

$$\dot{\omega}_1 = \frac{d}{dt}(\omega_1) \tag{17}$$

Acceleration vector of the end of the link and the center of link are calculated from equation (11, 12), and becomes

$$a_{e,1} = \dot{\omega}_1 \times r_{0,1} + \omega_1 \times (\omega_1 \times v_{0,1}) \tag{18}$$

$$a_{c,1} = \dot{\omega}_1 \times r_{0,c1} + \omega_1 \times (\omega_1 \times v_{0,c1}) \tag{19}$$

For lower boom (link 2),)

$$\omega_2 = {}^{2}\mathrm{R}_1\, \omega_1 + z_2\, \dot{\theta}_2 \tag{20}$$

$$\dot{\omega}_2 = \frac{d}{dt}(\omega_2) \tag{21}$$

$$a_{e,2} = {}^{2}\mathrm{R}_1\, a_{e,1} + \dot{\omega}_2 \times v_{1,2} + \omega_2 \times (\omega_2 \times v_{1,2}) \tag{22}$$

$$a_{c,2} = {}^{2}\mathrm{R}_1\, a_{e,1} + \dot{\omega}_2 \times v_{1,c2} + \omega_2 \times (\omega_2 \times v_{1,c2}) \tag{23}$$

For upper boom with an extension boom (link 3),

$$\omega_3 = {}^{3}\mathrm{R}_2\, \omega_2 + z_3\, \dot{\theta}_3 \tag{24}$$

$$\dot{\omega}_3 = \frac{d}{dt}(\omega_3) \tag{25}$$

$$a_{e,3} = {}^{3}\mathrm{R}_2\, a_{e,2} + \dot{\omega}_3 \times v_{2,3} + \omega_3 \times (\omega_3 \times v_{2,3}) \tag{26}$$

$$a_{c,3} = {}^{3}\mathrm{R}_2\, a_{e,2} + \dot{\omega}_3 \times v_{2,c3} + \omega_3 \times (\omega_3 \times v_{2,c3}) \tag{27}$$

For the bucket (link 4),

$$\omega_4 = {}^{4}\mathrm{R}_3\, \omega_3 + z_4\, \dot{\theta}_4 \tag{28}$$

$$\dot{\omega}_4 = \frac{d}{dt}(\omega_4) \tag{29}$$

$$a_{e,4} = {}^{4}\mathrm{R}_3\, a_{e,3} + \dot{\omega}_4 \times v_{3,4} + \omega_4 \times (\omega_4 \times v_{3,4}) \tag{30}$$

$$a_{c,4} = {}^{4}\mathrm{R}_3\, a_{e,3} + \dot{\omega}_4 \times v_{3,c4} + \omega_4 \times (\omega_4 \times v_{3,c4}) \tag{31}$$

Inward recursion for dynamics, starting from bucket to turntable:

For Bucket (link 4),

As previously described in assumption that the boom equipment is moving in a free space, so no external forces and torques are applied at the end of bucket i.e., $f_5 = \tau_5 = 0$.

The gravity vector is defined as

$$g_4 = {}^{4}\mathrm{R}_0\, g_0 \tag{32}$$

where, g_0 is the gravity vector defined in fixed frame as

$$g_0 = \begin{bmatrix} 0 \\ 0 \\ -g \end{bmatrix} \tag{33}$$

$$f_4 = m_4 a_{c,4} - m_4 g_4 \tag{34}$$

$$\tau_4 = -f_4 \times v_{3,c4} + \omega_4 \times (I_4\omega_4) + I_4\dot{\omega}_4 \tag{35}$$

For upper boom with an extension boom (link 3),

$$g_3 = {}^{3}\mathrm{R}_0\, g_0 \tag{36}$$

$$f_3 = {}^{3}\mathrm{R}_4\, f_4 + m_3 a_{c,3} - m_3 g_3 \tag{37}$$

$$\tau_3 = {}^{3}\mathrm{R}_4\, \tau_4 - f_3 \times v_{2,c3} + ({}^{3}\mathrm{R}_4\, f_4) \times v_{3,c3} + \omega_3 \times (I_3\omega_3) + I_3\dot{\omega}_3 \tag{38}$$

For lower boom (link 2),

$$g_2 = {}^{2}\mathrm{R}_0\, g_0 \tag{39}$$

$$f_2 = {}^{2}\mathrm{R}_3\, f_3 + m_2 a_{c,2} - m_2 g_2 \tag{40}$$

$$\tau_2 = {}^{2}\mathrm{R}_3\, \tau_3 - f_2 \times v_{1,c2} + ({}^{2}\mathrm{R}_3\, f_3) \times v_{2,c2} + \omega_2 \times (I_2\omega_2) + I_2\dot{\omega}_2 \tag{41}$$

For turntable (link 1),

$$g_1 = {}^1\mathrm{R}_0\, g_0 \tag{42}$$

$$f_1 = {}^1\mathrm{R}_2\, f_2 + m_1 a_{c,1} - m_1 g_1 \tag{43}$$

$$\tau_1 = {}^1\mathrm{R}_2\, \tau_2 - f_1 \times v_{0,c1} + \left({}^1\mathrm{R}_2\, f_2\right) \times v_{1,c1} + \omega_1 \times \left(I_1 \omega_1\right) + I_1 \dot{\omega}_1 \tag{44}$$

The equation of motion in matrix form are expressed as

$$M(\theta)\ddot{\theta} + C\left(\theta, \dot{\theta}\right)\dot{\theta} + g(\theta) = \tau \tag{45}$$

where, M is a 4 × 4 inertia mass matrix, C includes the Coriolis and centrifugal terms, g includes the gravity terms and τ is the joint torque vector. It should be emphasized that the backward recursion of link 1 is directly dependent on all seven steps back to the forward recursion of link 1. Thus, τ_1 and f_1 results in a huge vector. The joint force and torque vectors acting at joint 1 in x, y and z directions are listed in Appendix A.

The Boom Equipment-Utility Truck Combined Dynamic Model A novel approach and a method are represented in this section to combine morphing dynamics of a multi-body combination of the boom equipment manipulator, and the utility truck. The expression for the force that the manipulator exerts at its fixed base i.e., pedestal, and hence on the utility truck can be derived from the expression f_1, that appears in the backward recursion of Newton-Euler equations. The definition of f_1 is defined as the force exerted on link 1 by link 0 (the fixed base) at the coordinate frame x_0, y_0, z_0 to support link 1 and the links above it and can be expressed as

$$f_0 = {}^0\mathrm{R}_1\, f_1 \tag{46}$$

Thus, the actual force exerted by the boom equipment manipulator on the utility truck is equal and opposite and can be expressed as

$$f_B = -f_0 \tag{47}$$

The moment generated by this force at the center of gravity of the utility truck is calculated from following equation

$$M_{fB} = l_4 \times f_B \tag{48}$$

where, l_4 is the pedestal height which is a position vector from the boom equipment mounting point to the utility truck's center of gravity.

The expression for the moment that the manipulator exerts at its fixed base i.e., pedestal, and hence on the utility truck can be derived from the expression τ_1, that appears in the backward recursion of Newton-Euler equations. The definition of τ_1 is defined as the moment exerted on link 1 by link 0 (the fixed base) at the coordinate frame x_0, y_0, z_0 and can be expressed as

$$\tau_0 = {}^0\mathrm{R}_1\, \tau_1 \tag{49}$$

Thus, the actual moment exerted by the boom equipment manipulator on the utility truck is equal and opposite to τ_0 and can be expressed as

$$M_{\tau B} = -\tau_0 \tag{50}$$

Therefore, the final expression for the force and total moment exerted by the boom equipment on the utility truck can be expressed as

$$\begin{bmatrix} f_B \\ M_B \end{bmatrix} = \begin{bmatrix} f_{Bx} \\ f_{By} \\ f_{Bz} \\ M_{fBx} + M_{\tau Bx} \\ M_{fBy} + M_{\tau By} \\ M_{\tau Bz} \end{bmatrix} \tag{51}$$

This 5-DOF morphing dynamics of the boom equipment manipulator is coupled with the 7-DOF conventional dynamics of the utility truck with sprung and unsprung masses, as shown in Figure 5 and 6. The 7-DOF conventional dynamics of the truck is explained in [19]. Thus, the conventional dynamics of the utility truck is not explained in this paper. The forces and moments exerted by the morphing boom equipment are applied at the utility truck's center of gravity, which majorly affects the normal reaction at all four wheels. Hence, the normal reaction can be managed by morphing the boom equipment. Finally, more traction/grip can be achieved by managing normal reactions at the wheels.

Simulations and Results

Simulation and results are only shown for the dynamics of the boom equipment manipulator and three forces and moments are simulated at the vehicle's center of gravity. Multi-body combination of the boom equipment manipulator, and the utility truck dynamics simulations are ongoing study. Maple software [20] is used to derive the second order dynamic differential equations of the boom equipment and then MATLAB conversion code is used in the end to convert expressions from Maple to MATLAB code. Certain quantities are redefined to be compatible with MATLAB. The dynamic

FIGURE 5 Representation of the boom equipment as three forces and moments

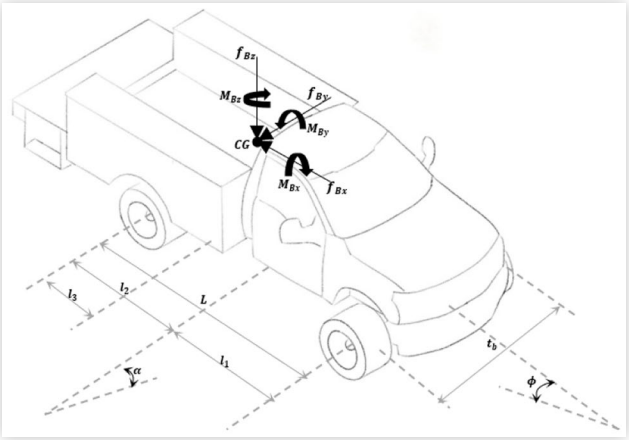

FIGURE 6 Integrated multi-body dynamics of the morphing boom equipment manipulator and the utility truck

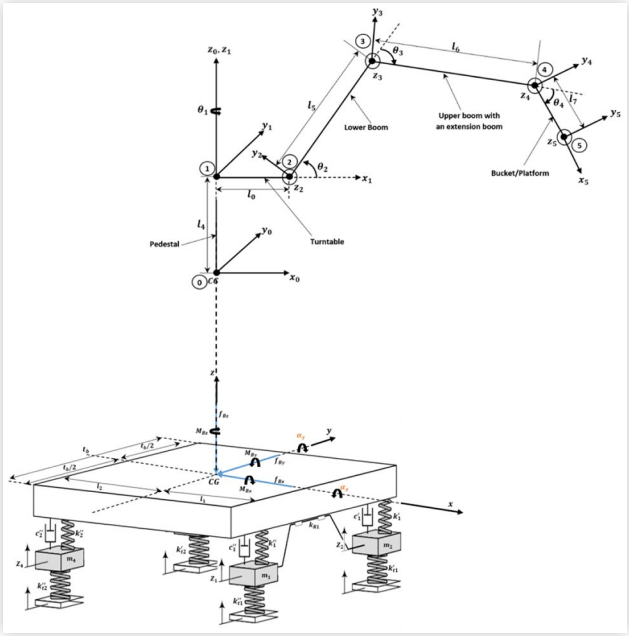

FIGURE 7 Simulink model with set-point feedback PD controller

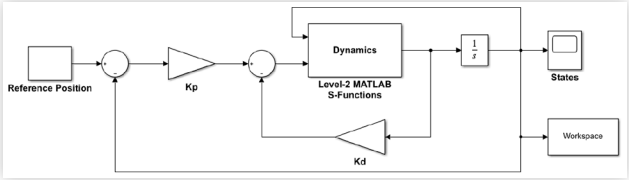

model of the boom equipment has been simulated in MATLAB and Simulink [21].

The ultimate goal of the simulations is to demonstrate that the boom equipment can morph from initial position A to reference position B. The feedback controllers continuously calculate the input joint toque at each step. In this study, the path is taken from position A to position B, and how long the motion will persist is not controlled in the set-point feedback controller. A simple PD controller is used for the position control of the system. An entire Simulink model with set-point feedback PD controller is shown in Figure 7. The Level-2 MATLAB S-Functions block is used in the Simulink model to implement the boom equipment dynamics, with input 1 as the state vector, input 2 as the applied torque vector, and output as the state derivatives vector. The ode45 (Dormand-Prince method) is used to solve the differential equation in Simulink with relative tolerance of 1e-8. The state vector is sent back to the MATLAB through To Workspace block from Simulink at each times step in the simulation to plot results graphically.

As described in previous section, the dynamic model of the boom equipment can be written on matrix form as

$$M(\theta)\ddot{\theta} + C(\theta,\dot{\theta})\dot{\theta} + g(\theta) = \tau \tag{52}$$

It is required in Simulink that the system must expressed in the first-order nonlinear form as

$$\dot{r} = f(\theta,\tau) \tag{53}$$

where r is the state vector and τ is the torque vector. The equation (52) becomes after rearranging the terms as follow

$$\ddot{\theta} = M^{-1}\left(-C\dot{\theta} - g + \tau\right) \tag{54}$$

An assumption is made that the inertia mass matrix M is invertible. The reason behind assuming is that the kinetic energy is always nonnegative. It is zero if and only if the velocity of all joints is zero. Therefore, M is considered invertible.

A simple PD controller scheme is used for the position control of the dynamic system described in equation (52) which can be proved in a Lyapunov stability as it is demonstrated in [22]. Each joint is controlled as an independent joint control i.e., single-input/single-output (SISO) system. The input torque vector can be written as

$$\tau = -K_p(\theta_{ref} - \theta) - K_d\dot{\theta} \tag{55}$$

where $(\theta_{ref} - \theta)$ is the error between the referenced joint value and the actual joint value, K_p and K_d are the PD controller parameter matrices of proportional and derivative gains. A set of propositional and derivative gain matrices are chosen as follows

$$K_p = \begin{bmatrix} 95000 & 0 & 0 & 0 \\ 0 & 85500 & 0 & 0 \\ 0 & 0 & 62000 & 0 \\ 0 & 0 & 0 & 37000 \end{bmatrix} [\text{Nm/rad}] \tag{56}$$

$$K_d = \begin{bmatrix} 85500 & 0 & 0 & 0 \\ 0 & 75250 & 0 & 0 \\ 0 & 0 & 66000 & 0 \\ 0 & 0 & 0 & 46500 \end{bmatrix} [\text{Nm/rad}] \tag{57}$$

Following are the reasons to select such a significant PD gain value,

- The dynamics of hydraulic actuators are not considered, since in general, it is not possible to specify actuator toques/forces in a hydraulic system.
- It can be used to evaluate the developed dynamic models and better understand the dynamic system behavior.
- Main objective of this study is to understand the multi-body dynamics of the boom equipment and the utility truck and how the normal reactions are changing at the wheels when the boom equipment manipulator morphs its orientation from position A to position B.
- Gain setting tune-up is the non-linear nature of the robot dynamics with varying inertia, which is more complex and thus, the gain tuning process becomes considerably more intricate in a linear setting.

- It is well known that high values of the proportional gain can obtain small position error.

A trial-and-error method was used to tune the controller's parameters; however, a more robust and accurate approach is needed when the manipulator moves from position A to position B in a precise fixed time interval. Therefore, a more suitable control strategy will be proposed in future studies.

The boom equipment is considered as a 5-DOF in this study. Hence, there are several possible orientations of the boom equipment to analyze the morphing dynamics of the boom equipment manipulator, which is very difficult to represent in this paper. However, all those possible morphing of the boom equipment can be done according to the requirements, out of which two simulations are presented here to evaluate the developed dynamic models and understand the dynamic system behavior.

Simulation 1

Reference position vector and initial conditions are set to

$$\theta_{initial} = [0 \;\; 0.261799 \;\; 0 \;\; 0] \tag{58}$$

$$\dot{\theta}_{initial} = [0 \quad 0 \quad 0 \quad 0] \tag{59}$$

$$\theta_{reference} = [1.0472 \quad 0.261799 \quad 0 \quad 0] \tag{60}$$

The response of joint angles, controlled input torque at each joint, moments and forces exerted by the boom equipment manipulator are shown in Figures 8, 9, 10, and 11 respectively.

Simulation 2

Reference position vector and initial conditions are set to

$$\theta_{initial} = [0.785398 \quad 0.261799 \quad 0 \quad 0] \tag{61}$$

$$\dot{\theta}_{initial} = [0 \quad 0 \quad 0 \quad 0] \tag{62}$$

$$\theta_{reference} = [0.785398 \quad 0.261799 \quad 0.523599 \quad 0] \tag{63}$$

The response of joint angles, controlled input torque at each joint, moments and forces exerted by the boom equipment manipulator are shown in Figures 12,13,14, and 15 respectively.

All the states converge to the reference value in about 4 seconds in simulations 1 and 2. The response of the system is very satisfying, and an asymptotic stability is verified in both the simulations.

FIGURE 8 Simulation 1: Response of joint angles

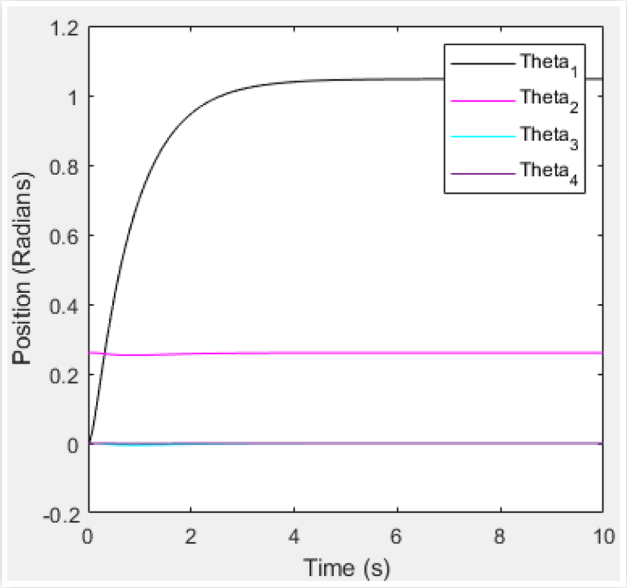

FIGURE 9 Simulation 1: Controlled input torque at each joint

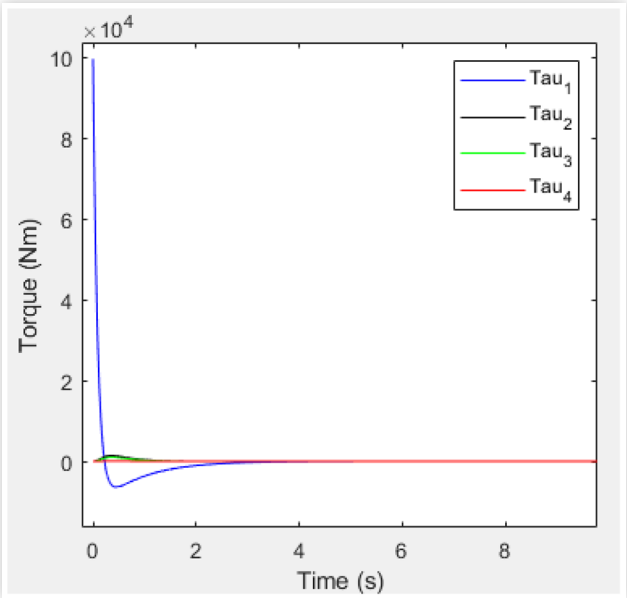

In simulation 1, the turntable angle (θ_1) morphs around *z*-axis from zero degree to 60^0, while other joints remain at its initial positions, as described in Table 1. It can be inferred from the practical consideration that this motion will produce a torque around *z* axis. It will exert a force and a moment at the vehicle's center of gravity in *x, y,* and *z* directions as shown in Figure 9,10, and 11 respectively. In simulation 2, the turntable angle (θ_1) is at 45^0, boom articulation angle (θ_3) morphs from zero degree to 30^0, and other joints remain at its initial position. The boom articulation angle gradually reaches its

FIGURE 10 Simulation 1: Total moments exerted by the boom equipment manipulator at the vehicle's center of gravity

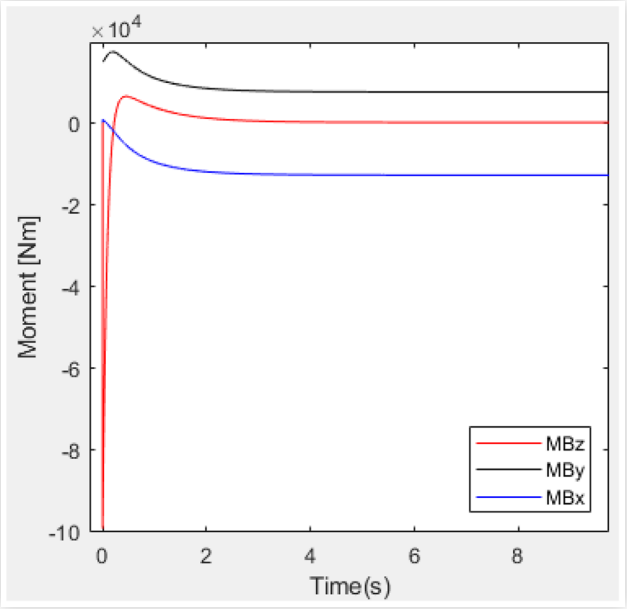

FIGURE 11 Simulation 1: Forces exerted by the boom equipment manipulator at the vehicle's center of gravity

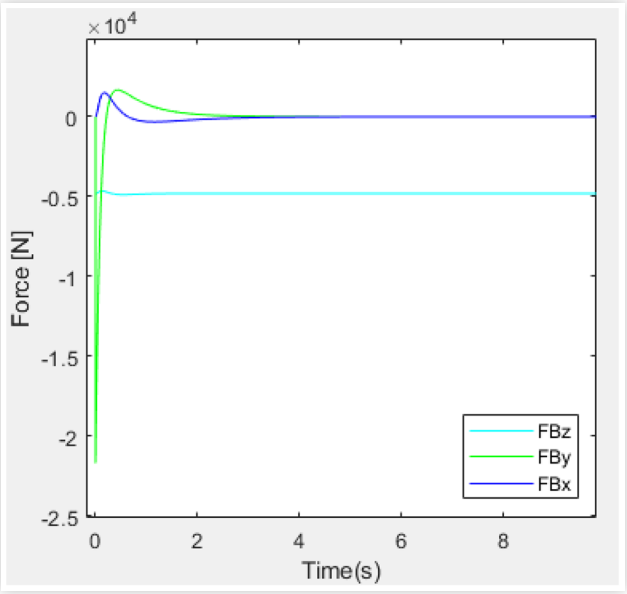

FIGURE 12 Simulation 2: Response of joint angles

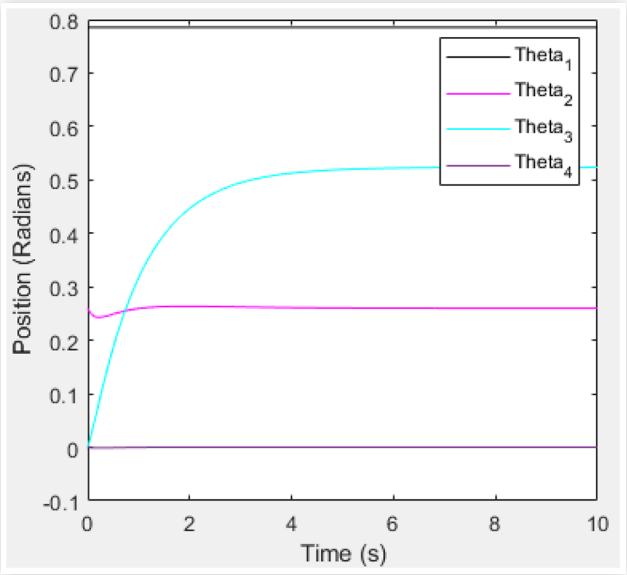

FIGURE 13 Simulation 2: Controlled input torque at each joint

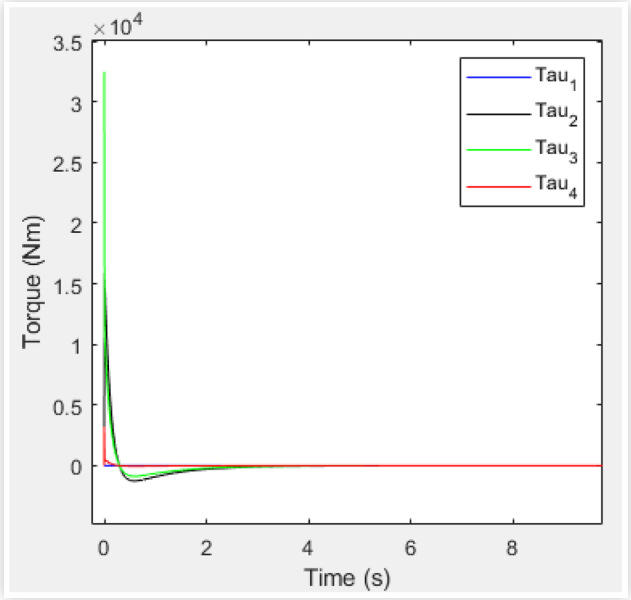

reference value, and the feedback controllers continuously calculates the input torque at each joint as shown in Figure 13. This motion exerts moments in x and y directions and forces in z and x directions at the vehicle's center of gravity as represented in Figures 14 and 15, respectively.

There are several control techniques and methodologies that exists and can be applied to control the manipulator according to the requirements for the robot manipulator operation.

Conclusions

In conclusion, the dynamic modeling of the morphing boom equipment is developed and implemented symbolically in compact form using the recursive Newton-Euler dynamical formulation in this paper. While the dynamics of the utility truck are conventional and thus, it is directly used to couple multibody dynamics of the boom equipment and the utility truck with sprung and unsprung masses. A novel approach, a method, and mathematical models are presented to investigate the dynamic coupling of the 5-DOF boom equipment

FIGURE 14 Simulation 2: Total moments exerted by the boom equipment manipulator at the vehicle's center of gravity

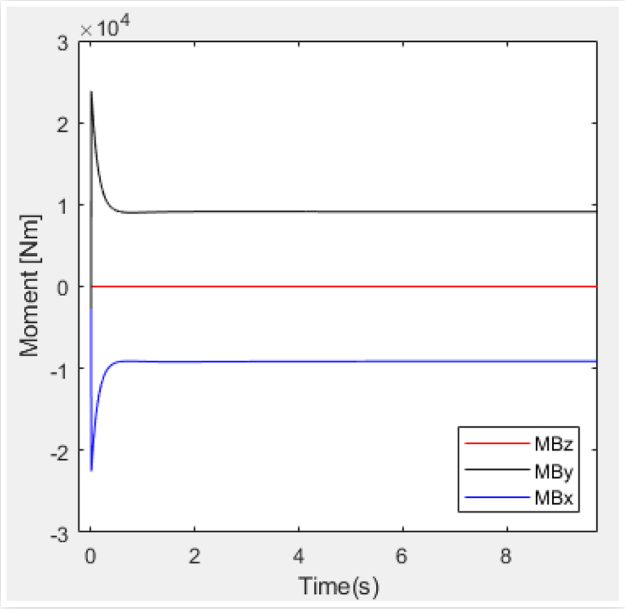

FIGURE 15 Simulation 2: Forces exerted by the boom equipment manipulator at the vehicle's center of gravity

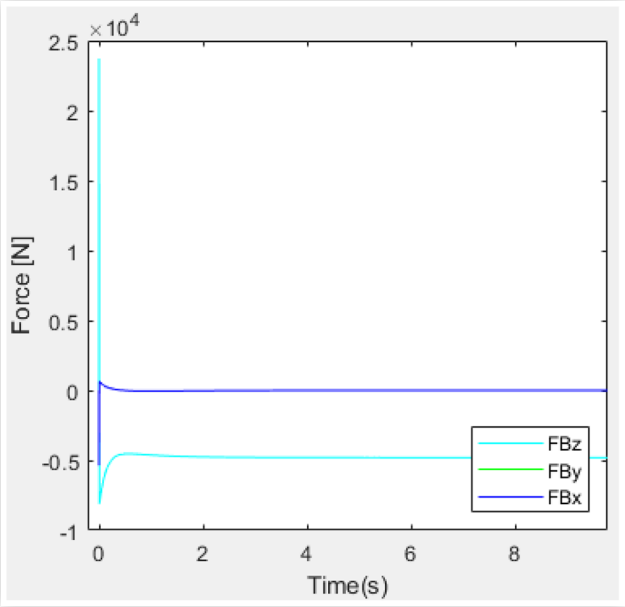

manipulator and the utility truck with 7-DOF conventional dynamics of sprung and unsprung masses. Simulation results of the morphing boom equipment's response were provided. Finally, forces and moments exerted by the morphing device at the vehicle's center of gravity were presented.

Future Work

The morphing of the boom equipment majorly impacts the normal reactions at all the wheels. Hence, the normal reaction can be managed by morphing the boom equipment and thus, more traction/grip can be achieved by managing normal reactions at the wheels .This multi-body combination of the boom equipment manipulator, and the utility truck conventional dynamics simulations are ongoing work which will be presented in a separate paper.

References

1. Li, Y., Xi, X., Xie, J. et al., "Study and Implementation of a Cooperative Hoisting for Two Crawler Cranes," *J Intell Robot Syst* 83 (2016): 165-178, doi:https://doi.org/10.1007/s10846-015-0296-x.
2. Eileen, H., "Dynamic Characterization and Analysis of Aerial Lifts," Master's Thesis, Georgia Institute of Technology, Atlanta, GA, 2012. http://hdl.handle.net/1853/45944.
3. Mijailović, R., "Modelling the Dynamic Behavior of the Truck-Crane," *Transport* 26, no. 4 (2011): 410-417, doi:https://doi.org/10.3846/16484142.2011.642946.
4. Fujioka, D., "Tip-Over Stability analysis for Mobile Boom Cranes with Single- and Double-Pendulum Payloads," Master's Thesis, Georgia Institute of Technology, Atlanta, GA, 2010. : http://hdl.handle.net/1853/37162.
5. Rauch, A., "Stability Analysis of Mobile Boom Cranes," Master's Thesis, Georgia Institute of Technology, Atlanta, GA, 2008. : http://hdl.handle.net/1853/26535.
6. Ehsan, M., "Dynamics and Control of a Small-Scale Mobile Boom Crane," Master's Thesis, Georgia Institute of Technology, Atlanta, GA, 2010. : http://hdl.handle.net/1853/37166.
7. Sheridan, T.B., *Telerobotics, Automation, and Human Supervisory Control* (The MIT Press, 1992)
8. Ashley, S.. "Underground Mining from Above," Mechanical Engineering-CIME, May 1995, 78+. Gale Academic OneFile (accessed October 12, 2021). https://link.gale.com/apps/doc/A17158422/AONE?u=anon~69183eca&sid=googleScholar&xid=76fde0ea.
9. Seward, D., "LUCIE- The Autonomous Robot Excavator," *Industrial Robots* 19, no. 1 (1992): 14-18.
10. Skibniewski, M.J., *Robotics in Civil Engineering*, Computational Mechanics Publications. Van Nostrand Reinhold, 1988, pp. 10- 13.
11. "Freight Facts and Figures 2015, US Department of Transportation, Bureau of Transportation Statistics," : http://www.princeton.edu/~alaink/Orf467F16/FHWA2201FreightFactsF_complete.pdf/
12. "Altec At200A Telescopic Aerial Device." https://www.altec.com/products/aerials/telescopic/at200a
13. Denavit, J. and Hartenberg, R.S., "A Kinematic Notation for Lower-Pair Mechanisms Based on Matrices," *Journal of Applied Mechanics* (1955): 215-221, doi:https://doi.org/10.1115/1.4011045.
14. Craig, J.J., *Introduction to Robotics*, 2nd ed. (Reading, MA: Addison-Wesley, 1989)

15. Luh, J.Y.S., Walker, M., and Paul, R.P., "On- Line Computational Scheme for Mechanical Manipulators," *J. of Dynamic Systems, Measurement and Control* 102 (1980): 69-76, doi:https://doi.org/10.1115/1.3149599.
16. Sarkar, S., "Dynamic Modeling of an Articulated Forestry Machine for Simulation and Control," Master's Thesis, McGill University, 1996. : https://escholarship.mcgill.ca/concern/theses/j9602285v
17. Vaha, P. and Skibniewski, M., "Dynamic model of an excavator," *Journal of Aerospace Engineering* 6 (1993): 148-158, doi:https://doi.org/10.1061/(ASCE)0893-1321(1993)6:2(148).
18. Koivo, A., "Kinematics of Excavator (Backhoes) for Transferring Surface Material," *Journal of Aerospace Engineering* 7 (1994): 17-31, doi:https://doi.org/10.1061/(ASCE)0893-1321(1994)7:1(17).
19. Jazar, R.N., "Vehicle Vibrations," in: , *Vehicle Dynamics: Theory and Application*, (Springer, 2008), 827-881.
20. Maple (2019). Maplesoft, a Division of Waterloo Maple Inc., Waterloo, Ontario.
21. MATLAB and Statistics Toolbox Release R2020b, The MathWorks, Inc., Natick, Massachusetts, United States.
22. Sciavicco, L. and Siciliano, B., *Modelling and Control of Robot Manipulators* (Springer Verlag, 2000)

Contact Information

Contact author name: Parth Y. Patel
University of Alabama at Birmingham
parth144@uab.edu

Acknowledgments

This research is supported by NSF award S&AS-1849264. We would like to express our gratefulness to Altec Inc., our research partner for providing utility truck and required data for the research analysis, which aided us to progress in our research.

Abbreviations

DOF - degree of freedom

A-IMS - Aerodynamic Intelligent Morphing System

PD - proportional derivative

D-H - Denavit-Hartenberg

SISO - single-input/single-output

Nomenclatures

$\boldsymbol{\theta_i}$ - joint variable angle of link *i*

$\boldsymbol{l_0}$ - turntable length

$\boldsymbol{l_4}$ - pedestal height

$\boldsymbol{l_5}$ - lower boom length

$\boldsymbol{l_6}$ - upper boom with an extension length

$\boldsymbol{l_7}$ - bucket length

$\boldsymbol{a_{c,i}}$ - linear acceleration vector of the center of mass of link *i*.

$\boldsymbol{a_{e,i}}$ - linear acceleration vector of the end of link *i* in coordinate frame *i*.

$\boldsymbol{\omega_i}$ - angular velocity vector of link *i* with respect to frame 0.

$\dot{\boldsymbol{\omega}}_i$ - angular acceleration vector of link *i* with respect to frame 0.

$\boldsymbol{g_i}$ - acceleration due to gravity

$\boldsymbol{m_i}$ - mass of link *i*

$\boldsymbol{I_i}$ - inertia tensor of link *i* with respect to the center of mass of link *i* expressed in a frame located at the center of mass of the link *i*.

$\boldsymbol{v_{i\text{-}1,ci}}$ - position vector from the origin of frame (*i*-1) to the center of mass of link *i*.

$\boldsymbol{v_{i\text{-}1,ci}}$ - position vector from the origin of frame (*i*-1) to the origin of frame *i*.

$\boldsymbol{v_{i\text{-}1,i}}$ - position vector from the origin of frame (*i*-1) to the origin of frame *i*.

$\boldsymbol{v_{i,ci}}$ - position vector from the origin of frame *i* to the center of mass of link *i*

${}^{\boldsymbol{i}}\mathbf{R}_{\boldsymbol{i+1}}$ - rotation matrix from frame *i* to frame (*i*+1)

$\boldsymbol{z_i}$ - rotation of joint *i* expressed in frame *i*

$\boldsymbol{M}$ - inertia mass matrix

$\boldsymbol{C}$ - Coriolis and centrifugal terms

$\boldsymbol{\tau}$ - joint torque vector

$\boldsymbol{K_p}$ - PD controller proportional gain

$\boldsymbol{K_d}$ - PD controller derivative gain.

Appendix A

Expression of Force and Torque Vectors Acting at Joint 1 in x, y, and z Directions

In the following expressions, diff(diff(θ_i(t), t), t) represents $\ddot{\theta}_i(t)$ and diff(θ_i(t), t)) represents $\dot{\theta}_i(t)$.

τ_{1z} =(m4 * l7 ^ 2 / 0.8e1 + I2yy / 0.2e1 + I2xx / 0.2e1 + m2 * l5 ^ 2 / 0.8e1 + l5 ^ 2 * m3 / 0.2e1 + l5 ^ 2 * m4 / 0.2e1 + l7 * m4 * cos(θ4(t)) * l6 / 0.2e1 + l7 * m4 * l5 * cos(θ4(t) + θ3(t)) / 0.2e1 + cos(θ3(t)) * l5 * l6 * m4 + l6 * m3 * cos(θ3(t)) * l5 / 0.2e1 + I4xx / 0.2e1 + I4yy / 0.2e1 + I1zz + m4 * l0 ^ 2 + m3 * l0 ^ 2 + m2 * l0 ^ 2 + m1 * l0 ^ 2 / 0.4e1 - I2xx * cos((2 * θ2(t))) / 0.2e1 + I3yy * cos((2 * θ2(t)) + 0.2e1 * θ3(t)) / 0.2e1 - I3xx * cos((2 * θ2(t)) + 0.2e1 * θ3(t)) / 0.2e1 - I4xx * cos((2 * θ2(t)) + 0.2e1 * θ3(t) + 0.2e1 * θ4(t)) / 0.2e1 + I4yy * cos((2 * θ2(t)) + 0.2e1 * θ3(t) + 0.2e1 * θ4(t)) / 0.2e1 + I2yy * cos((2 * θ2(t))) / 0.2e1 + I3yy / 0.2e1 + I3xx / 0.2e1 + l5 * l6 * m3 * cos(θ3(t) + (2 * θ2(t))) / 0.2e1 + l5 * l6 * m4 * cos(θ3(t) + (2 * θ2(t))) + l5 * l7 * m4 * cos(θ4(t) + θ3(t) + (2 * θ2(t))) / 0.2e1 + l6 * l7 * m4 * cos(θ4(t) + (2 * θ2(t)) + 0.2e1 * θ3(t)) / 0.2e1 + 0.2e1 * cos(θ2(t)) * l5 * m4 * l0 + 0.2e1 * cos(θ2(t)) * l5 * m3 * l0 + cos(θ2(t)) * l5 * m2 * l0 + l0 * m4 * cos(θ2(t) + θ3(t) + θ4(t)) * l7 + 0.2e1 * l0 * m4 * cos(θ2(t) + θ3(t)) * l6 + l0 * m3 * cos(θ2(t) + θ3(t)) * l6 + l7 ^ 2 * m4 * cos((2 * θ2(t)) + 0.2e1 * θ3(t) + 0.2e1 * θ4(t)) / 0.8e1 + l6 ^ 2 * m3 * cos((2 * θ2(t)) + 0.2e1 * θ3(t)) / 0.8e1 + l6 ^ 2 * m4 * cos((2 * θ2(t)) + 0.2e1 * θ3(t)) / 0.2e1 + m4 * l5 ^ 2 * cos((2 * θ2(t))) / 0.2e1 + m3 * l5 ^ 2 * cos((2 * θ2(t))) / 0.2e1 + m2 * l5 ^ 2 * cos((2 * θ2(t))) / 0.8e1 + m3 * l6 ^ 2 / 0.8e1 + l6 ^ 2 * m4 / 0.2e1) * diff(diff(θ1(t), t), t) + ((-sin((2 * θ2(t))) * l5 ^ 2 * m4 - sin((2 * θ2(t))) * l5 ^ 2 * m3 - m2 * l5 ^ 2 * sin((2 * θ2(t))) / 0.4e1 - sin((2 * θ2(t)) + 0.2e1 * θ3(t)) * l6 ^ 2 * m4 - m4 * l7 ^ 2 * sin((2 * θ2(t)) + 0.2e1 * θ3(t) + 0.2e1 * θ4(t)) / 0.4e1 - m3 * l6 ^ 2 * sin((2 * θ2(t)) + 0.2e1 * θ3(t)) / 0.4e1 - I3yy * sin((2 * θ2(t)) + 0.2e1 * θ3(t)) - I4yy * sin((2 * θ2(t)) + 0.2e1 * θ3(t) + 0.2e1 * θ4(t)) + I2xx * sin((2 * θ2(t))) - I2yy * sin((2 * θ2(t))) + I4xx * sin((2 * θ2(t)) + 0.2e1 * θ3(t) + 0.2e1 * θ4(t)) + I3xx * sin((2 * θ2(t)) + 0.2e1 * θ3(t)) - 0.2e1 * sin(θ2(t) + θ3(t)) * l0 * l6 * m4 - 0.2e1 * sin(θ2(t)) * l0 * l5 * m4 - l6 * m3 * l0 * sin(θ2(t) + θ3(t)) - 0.2e1 * sin(θ2(t)) * l0 * l5 * m3 - l5 * m2 * sin(θ2(t)) * l0 - 0.2e1 * sin(θ3(t) + (2 * θ2(t))) * l5 * l6 * m4 - l7 * m4 * l5 * sin(θ4(t) + θ3(t) + (2 * θ2(t))) - l7 * m4 * l6 * sin(θ4(t) + (2 * θ2(t)) + 0.2e1 * θ3(t)) - l6 * m3 * l5 * sin(θ3(t) + (2 * θ2(t))) - l7 * m4 * l0 * sin(θ2(t) + θ3(t) + θ4(t))) * diff(θ2(t), t) + (-m3 * l6 ^ 2 * sin((2 * θ2(t)) + 0.2e1 * θ3(t)) / 0.4e1 - sin((2 * θ2(t)) + 0.2e1 * θ3(t)) * l6 ^ 2 * m4 - m4 * l7 ^ 2 * sin((2 * θ2(t)) + 0.2e1 * θ3(t) + 0.2e1 * θ4(t)) / 0.4e1 + I3xx * sin((2 * θ2(t)) + 0.2e1 * θ3(t)) - I3yy * sin((2 * θ2(t)) + 0.2e1 * θ3(t)) + I4xx * sin((2 * θ2(t)) + 0.2e1 * θ3(t) + 0.2e1 * θ4(t)) - I4yy * sin((2 * θ2(t)) + 0.2e1 * θ3(t) + 0.2e1 * θ4(t)) - l7 * m4 * l0 * sin(θ2(t) + θ3(t) + θ4(t)) - 0.2e1 * sin(θ2(t) + θ3(t)) * l0 * l6 * m4 - l6 * m3 * l0 * sin(θ2(t) + θ3(t)) - l7 * m4 * l6 * sin(θ4(t) + (2 * θ2(t)) + 0.2e1 * θ3(t)) - l7 * m4 * l5 * sin(θ4(t) + θ3(t) + (2 * θ2(t))) / 0.2e1 - l7 * m4 * l5 * sin(θ4(t) + θ3(t)) / 0.2e1 - sin(θ3(t) + (2 * θ2(t))) * l5 * l6 * m4 - sin(θ3(t)) * l5 * l6 * m4 - l6 * m3 * l5 * sin(θ3(t) + (2 * θ2(t))) / 0.2e1 - l6 * m3 * sin(θ3(t)) * l5 / 0.2e1) * diff(θ3(t), t) + (-m4 * l7 ^ 2 * sin((2 * θ2(t)) + 0.2e1 * θ3(t) + 0.2e1 * θ4(t)) / 0.4e1 - I4yy * sin((2 * θ2(t)) + 0.2e1 * θ3(t) + 0.2e1 * θ4(t)) + I4xx * sin((2 * θ2(t)) + 0.2e1 * θ3(t) + 0.2e1 * θ4(t)) - l7 * m4 * sin(θ4(t)) * l6 / 0.2e1 - l7 * m4 * l6 * sin(θ4(t) + (2 * θ2(t)) + 0.2e1 * θ3(t)) / 0.2e1 - l7 * m4 * l5 * sin(θ4(t) + θ3(t) + (2 * θ2(t))) / 0.2e1 - l7 * m4 * l5 * sin(θ4(t) + θ3(t)) / 0.2e1 - l7 * m4 * l0 * sin(θ2(t) + θ3(t) + θ4(t))) * diff(θ4(t), t)) * diff(θ1(t), t);

τ_{1y} = (-l5 ^ 2 * m3 - l5 ^ 2 * m4 - cos(θ2(t)) * l5 * m2 * l0 / 0.2e1 - l6 ^ 2 * m4 - m4 * l7 ^ 2 / 0.4e1 - m3 * l6 ^ 2 / 0.4e1 - m2 * l5 ^ 2 / 0.4e1 - l0 * m4 * cos(θ2(t) + θ3(t) + θ4(t)) * l7 / 0.2e1 - cos(θ2(t)) * l5 * m3 * l0 - cos(θ2(t)) * l5 * m4 * l0 - l0 * m3 * cos(θ2(t) + θ3(t)) * l6 / 0.2e1 - l0 * m4 * cos(θ2(t) + θ3(t)) * l6 - I2zz - 0.2e1 * cos(θ3(t)) * l5 * l6 * m4 - I4zz - I3zz - l6 * m3 * cos(θ3(t)) * l5 - l7 * m4 * cos(θ4(t)) * l6 - l7 * m4 * l5 * cos(θ4(t) + θ3(t))) * diff(diff(θ2(t), t), t) + (-l6 ^ 2 * m4 - m4 * l7 ^ 2 / 0.4e1 - m3 * l6 ^ 2 / 0.4e1 - l0 * m4 * cos(θ2(t) + θ3(t) + θ4(t)) * l7 / 0.2e1 - l0 * m3 * cos(θ2(t) + θ3(t)) * l6 / 0.2e1 - l0 * m4 * cos(θ2(t) + θ3(t)) * l6 - cos(θ3(t)) * l5 * l6 * m4 - l7 * m4 * l5 * cos(θ4(t) + θ3(t)) / 0.2e1 - l6 * m3 * cos(θ3(t)) * l5 / 0.2e1 - I4zz - I3zz - l7 * m4 * cos(θ4(t)) * l6) * diff(diff(θ3(t), t), t) + (-m4 * l7 ^ 2 / 0.4e1 - l0 * m4 * cos(θ2(t) + θ3(t) + θ4(t)) * l7 / 0.2e1 - l7 * m4 * l5 * cos(θ4(t) + θ3(t)) / 0.2e1 - I4zz - l7 * m4 * cos(θ4(t)) * l6 / 0.2e1) * diff(diff(θ4(t), t), t) + (-m4 * l7 ^ 2 * sin(0.2e1 * θ2(t) + 0.2e1 * θ3(t) + 0.2e1 * θ4(t)) / 0.8e1 - m3 * l6 ^ 2 * sin(0.2e1 * θ2(t) + 0.2e1 * θ3(t)) / 0.8e1 - m2 * l5 ^ 2 * sin(0.2e1 * θ2(t)) / 0.8e1 - sin(0.2e1 * θ2(t)) * l5 ^ 2 * m3 / 0.2e1 - sin(0.2e1 * θ2(t)) * l5 ^ 2 * m4 / 0.2e1 - I2yy * sin(0.2e1 * θ2(t)) / 0.2e1 + I2xx * sin(0.2e1 * θ2(t)) / 0.2e1 - sin(θ2(t)) * l0 * l5 * m3 - sin(θ2(t)) * l0 * l5 * m4 - sin(θ2(t) + θ3(t)) * l0 * l6 * m4 - sin(θ3(t) + 0.2e1 * θ2(t)) * l5 * l6 * m4 - l5 * m2 * sin(θ2(t)) * l0 / 0.2e1 - sin(0.2e1 * θ2(t) + 0.2e1 * θ3(t)) * l6 ^ 2 * m4 / 0.2e1 - l6 * m3 * l0 * sin(θ2(t) + θ3(t)) / 0.2e1 - l6 * m3 * l5 * sin(θ3(t) + 0.2e1 * θ2(t)) / 0.2e1 - l7 * m4 * l6 * sin(θ4(t) + 0.2e1 * θ2(t) + 0.2e1 * θ3(t)) / 0.2e1 - l7 * m4 * l0 * sin(θ2(t) + θ3(t) + θ4(t)) / 0.2e1 - l7 * m4 * l5 * sin(θ4(t) + θ3(t) + 0.2e1 * θ2(t)) / 0.2e1 - I3yy * sin(0.2e1 * θ2(t) + 0.2e1 * θ3(t)) / 0.2e1 + I3xx * sin(0.2e1 * θ2(t) + 0.2e1 * θ3(t)) / 0.2e1 - I4yy * sin(0.2e1 * θ2(t) + 0.2e1 * θ3(t) + 0.2e1 * θ4(t)) / 0.2e1 + I4xx * sin(0.2e1 * θ2(t) + 0.2e1 * θ3(t) + 0.2e1 * θ4(t)) / 0.2e1) * diff(θ1(t), t) ^ 2 + (l5 * m2 * sin(θ2(t)) * l0 / 0.2e1 + l7 * m4 * l0 * sin(θ2(t) + θ3(t) + θ4(t)) / 0.2e1 + l6 * m3 * l0 * sin(θ2(t) + θ3(t)) / 0.2e1 + sin(θ2(t) + θ3(t)) * l0 * l6 * m4 + sin(θ2(t)) * l0 * l5 * m3 + sin(θ2(t)) * l0 * l5 * m4) * diff(θ2(t), t) ^ 2 + ((l7 * m4 * l5 * sin(θ4(t) + θ3(t)) + l7 * m4 * l0 *

sin(θ2(t) + θ3(t) + θ4(t)) + l6 * m3 * l0 * sin(θ2(t) + θ3(t)) + 0.2e1 * sin(θ2(t) + θ3(t)) * l0 * l6 * m4 + l6 * m3 * sin(θ3(t)) * l5 + 0.2e1 * sin(θ3(t)) * l5 * l6 * m4) * diff(θ3(t), t) + (l7 * m4 * l5 * sin(θ4(t) + θ3(t)) + l7 * m4 * l0 * sin(θ2(t) + θ3(t) + θ4(t)) + l7 * m4 * sin(θ4(t)) * l6) * diff(θ4(t), t)) * diff(θ2(t), t) + (l7 * m4 * l0 * sin(θ2(t) + θ3(t) + θ4(t)) / 0.2e1 + l6 * m3 * l0 * sin(θ2(t) + θ3(t)) / 0.2e1 + sin(θ2(t) + θ3(t)) * l0 * l6 * m4 + l7 * m4 * l5 * sin(θ4(t) + θ3(t)) / 0.2e1 + sin(θ3(t)) * l5 * l6 * m4 + l6 * m3 * sin(θ3(t)) * l5 / 0.2e1) * diff(θ3(t), t) ^ 2 + (l7 * m4 * l5 * sin(θ4(t) + θ3(t)) + l7 * m4 * l0 * sin(θ2(t) + θ3(t) + θ4(t)) + l7 * m4 * sin(θ4(t)) * l6) * diff(θ4(t), t) * diff(θ3(t), t) + (l7 * m4 * l0 * sin(θ2(t) + θ3(t) + θ4(t)) / 0.2e1 + l7 * m4 * l5 * sin(θ4(t) + θ3(t)) / 0.2e1 + l7 * m4 * sin(θ4(t)) * l6 / 0.2e1) * diff(θ4(t), t) ^ 2 - l7 * m4 * cos(θ2(t) + θ3(t) + θ4(t)) * g / 0.2e1 - l6 * m3 * cos(θ2(t) + θ3(t)) * g / 0.2e1 - l5 * m2 * cos(θ2(t)) * g / 0.2e1 - cos(θ2(t)) * g * l5 * m3 - cos(θ2(t)) * g * l5 * m4 - l0 * m1 * g / 0.2e1 - g * l0 * m2 - g * l0 * m3 - g * l0 * m4 - cos(θ2(t) + θ3(t)) * g * l6 * m4;

τ_{1x} = (-m4 * l7 ^ 2 * sin((2 * θ2(t) + 2 * θ3(t) + 2 * θ4(t))) / 0.8e1 - m3 * l6 ^ 2 * sin((2 * θ2(t) + 2 * θ3(t))) / 0.8e1 - m2 * l5 ^ 2 * sin((2 * θ2(t))) / 0.8e1 - sin((2 * θ2(t))) * l5 ^ 2 * m3 / 0.2e1 - sin((2 * θ2(t))) * l5 ^ 2 * m4 / 0.2e1 - I2yy * sin((2 * θ2(t))) / 0.2e1 + I2xx * sin((2 * θ2(t))) / 0.2e1 - sin(θ2(t)) * l0 * l5 * m3 - sin(θ2(t)) * l0 * l5 * m4 - sin((θ2(t) + θ3(t))) * l0 * l6 * m4 - sin((θ3(t) + 2 * θ2(t))) * l5 * l6 * m4 - l5 * m2 * sin(θ2(t)) * l0 / 0.2e1 - sin((2 * θ2(t) + 2 * θ3(t))) * l6 ^ 2 * m4 / 0.2e1 - l6 * m3 * l0 * sin((θ2(t) + θ3(t))) / 0.2e1 - l6 * m3 * l5 * sin((θ3(t) + 2 * θ2(t))) / 0.2e1 - l7 * m4 * l6 * sin((θ4(t) + 2 * θ2(t) + 2 * θ3(t))) / 0.2e1 - l7 * m4 * l0 * sin((θ2(t) + θ3(t) + θ4(t))) / 0.2e1 - l7 * m4 * l5 * sin((θ4(t) + θ3(t) + 2 * θ2(t))) / 0.2e1 - I3yy * sin((2 * θ2(t) + 2 * θ3(t))) / 0.2e1 + I3xx * sin((2 * θ2(t) + 2 * θ3(t))) / 0.2e1 - I4yy * sin((2 * θ2(t) + 2 * θ3(t) + 2 * θ4(t))) / 0.2e1 + I4xx * sin((2 * θ2(t) + 2 * θ3(t) + 2 * θ4(t))) / 0.2e1) * diff(diff(θ1(t), t), t) + ((m4 * l7 ^ 2 / 0.4e1 + I2zz + m2 * l5 ^ 2 / 0.4e1 + l5 ^ 2 * m3 + l5 ^ 2 * m4 + l7 * m4 * cos(θ4(t)) * l6 + l7 * m4 * l5 * cos((θ4(t) + θ3(t))) + 0.2e1 * cos(θ3(t)) * l5 * l6 * m4 + l6 * m3 * cos(θ3(t)) * l5 + I4zz + I2xx * cos((2 * θ2(t))) - I3yy * cos((2 * θ2(t) + 2 * θ3(t))) + I3xx * cos((2 * θ2(t) + 2 * θ3(t))) + I4xx * cos((2 * θ2(t) + 2 * θ3(t) + 2 * θ4(t))) - I4yy * cos((2 * θ2(t) + 2 * θ3(t) + 2 * θ4(t))) - I2yy * cos((2 * θ2(t))) + I3zz - l5 * l6 * m3 * cos((θ3(t) + 2 * θ2(t))) - 0.2e1 * l5 * l6 * m4 * cos((θ3(t) + 2 * θ2(t))) - l5 * l7 * m4 * cos((θ4(t) + θ3(t) + 2 * θ2(t))) - l6 * l7 * m4 * cos((θ4(t) + 2 * θ2(t) + 2 * θ3(t))) - l7 ^ 2 * m4 * cos((2 * θ2(t) + 2 * θ3(t) + 2 * θ4(t))) / 0.4e1 - l6 ^ 2 * m3 * cos((2 * θ2(t) + 2 * θ3(t))) / 0.4e1 - l6 ^ 2 * m4 * cos((2 * θ2(t) + 2 * θ3(t))) - m4 * l5 ^ 2 * cos((2 * θ2(t))) - m3 * l5 ^ 2 * cos((2 * θ2(t))) - m2 * l5 ^ 2 * cos((2 * θ2(t))) / 0.4e1 + m3 * l6 ^ 2 / 0.4e1 + l6 ^ 2 * m4) * diff(θ2(t), t) + (l7 * m4 * l5 * cos((θ4(t) + θ3(t))) / 0.2e1 - l5 * l7 * m4 * cos((θ4(t) + θ3(t) + 2 * θ2(t))) / 0.2e1 + l6 * m3 * cos(θ3(t)) * l5 / 0.2e1 - l5 * l6 * m3 * cos((θ3(t) + 2 * θ2(t))) / 0.2e1 + cos(θ3(t)) * l5 * l6 * m4 - l5 * l6 * m4 * cos((θ3(t) + 2 * θ2(t))) + l7 * m4 * cos(θ4(t)) * l6 - l6 * l7 * m4 * cos((θ4(t) + 2 * θ2(t) + 2 * θ3(t))) - l7 ^ 2 * m4 * cos((2 * θ2(t) + 2 * θ3(t) + 2 * θ4(t))) / 0.4e1 - l6 ^ 2 * m3 * cos((2 * θ2(t) + 2 * θ3(t))) / 0.4e1 - l6 ^ 2 * m4 * cos((2 * θ2(t) + 2 * θ3(t))) - I4yy * cos((2 * θ2(t) + 2 * θ3(t) + 2 * θ4(t))) + I3xx * cos((2 * θ2(t) + 2 * θ3(t))) - I3yy * cos((2 * θ2(t) + 2 * θ3(t))) + m3 * l6 ^ 2 / 0.4e1 + l6 ^ 2 * m4 + I4zz + I3zz + m4 * l7 ^ 2 / 0.4e1 + I4xx * cos((2 * θ2(t) + 2 * θ3(t) + 2 * θ4(t)))) * diff(θ3(t), t) + (l7 * m4 * cos(θ4(t)) * l6 / 0.2e1 - l6 * l7 * m4 * cos((θ4(t) + 2 * θ2(t) + 2 * θ3(t))) / 0.2e1 + l7 * m4 * l5 * cos((θ4(t) + θ3(t))) / 0.2e1 - l5 * l7 * m4 * cos((θ4(t) + θ3(t) + 2 * θ2(t))) / 0.2e1 - l7 ^ 2 * m4 * cos((2 * θ2(t) + 2 * θ3(t) + 2 * θ4(t))) / 0.4e1 - I4yy * cos((2 * θ2(t) + 2 * θ3(t) + 2 * θ4(t))) + I4xx * cos((2 * θ2(t) + 2 * θ3(t))) + I4zz + m4 * l7 ^ 2 / 0.4e1) * diff(θ4(t), t)) * diff(θ1(t), t);

f_{1z} = (m2 * cos(θ2(t)) * l5 / 0.2e1 + m3 * cos(θ2(t) + θ3(t)) * l6 / 0.2e1 + cos(θ2(t) + θ3(t) + θ4(t)) * l7 * m4 / 0.2e1 + cos(θ2(t) + θ3(t)) * l6 * m4 + m3 * cos(θ2(t)) * l5 + cos(θ2(t)) * l5 * m4) * diff(diff(θ2(t), t), t) + (m3 * cos(θ2(t) + θ3(t)) * l6 / 0.2e1 + cos(θ2(t) + θ3(t) + θ4(t)) * l7 * m4 / 0.2e1 + cos(θ2(t) + θ3(t)) * l6 * m4) * diff(diff(θ3(t), t), t) + m4 * l7 * diff(diff(θ4(t), t), t) * cos(θ2(t) + θ3(t) + θ4(t)) / 0.2e1 + (-sin(θ2(t)) * l5 * m2 / 0.2e1 - sin(θ2(t) + θ3(t) + θ4(t)) * l7 * m4 / 0.2e1 - sin(θ2(t) + θ3(t)) * l6 * m4 - sin(θ2(t) + θ3(t)) * l6 * m3 / 0.2e1 - sin(θ2(t)) * l5 * m3 - sin(θ2(t)) * l5 * m4) * diff(θ2(t), t) ^ 2 + ((-sin(θ2(t) + θ3(t) + θ4(t)) * l7 * m4 - sin(θ2(t) + θ3(t)) * l6 * m3 - 0.2e1 * sin(θ2(t) + θ3(t)) * l6 * m4) * diff(θ3(t), t) - diff(θ4(t), t) * sin(θ2(t) + θ3(t) + θ4(t)) * l7 * m4) * diff(θ2(t), t) + (-sin(θ2(t) + θ3(t) + θ4(t)) * l7 * m4 / 0.2e1 - sin(θ2(t) + θ3(t)) * l6 * m3 / 0.2e1 - sin(θ2(t) + θ3(t)) * l6 * m4) * diff(θ3(t), t) ^ 2 - m4 * diff(θ4(t), t) * diff(θ3(t), t) * l7 * sin(θ2(t) + θ3(t) + θ4(t)) + m2 * g + m4 * g + m3 * g + m1 * g - m4 * diff(θ4(t), t) ^ 2 * l7 * sin(θ2(t) + θ3(t) + θ4(t)) / 0.2e1;

f_{1y} = (cos(θ2(t) + θ3(t) + θ4(t)) * l7 * m4 / 0.2e1 + cos(θ2(t)) * l5 * m4 + cos(θ2(t) + θ3(t)) * l6 * m4 + l0 * m4 + m3 * cos(θ2(t)) * l5 + m3 * cos(θ2(t) + θ3(t)) * l6 / 0.2e1 + m3 * l0 + m2 * cos(θ2(t)) * l5 / 0.2e1 + m2 * l0 + m1 * l0 / 0.2e1) * diff(diff(θ1(t), t), t) + ((-sin(θ2(t)) * l5 * m2 - 0.2e1 * sin(θ2(t)) * l5 * m3 - 0.2e1 * sin(θ2(t)) * l5 * m4 - sin(θ2(t) + θ3(t) + θ4(t)) * l7 * m4 - sin(θ2(t) + θ3(t)) * l6 * m3 - 0.2e1 * sin(θ2(t) + θ3(t)) * l6 * m4) * diff(θ2(t), t) + (-sin(θ2(t) + θ3(t) + θ4(t)) * l7 * m4 - sin(θ2(t) + θ3(t)) * l6 * m3 - 0.2e1 * sin(θ2(t) + θ3(t)) * l6 * m4) * diff(θ3(t), t) - diff(θ4(t), t) * sin(θ2(t) + θ3(t) + θ4(t)) * l7 * m4) * diff(θ1(t), t);

f_{1x} = (-sin(θ2(t)) * l5 * m2 / 0.2e1 - sin(θ2(t) + θ3(t) + θ4(t)) * l7 * m4 / 0.2e1 - sin(θ2(t) + θ3(t)) * l6 * m4 - sin(θ2(t) + θ3(t)) * l6 * m3 / 0.2e1 - sin(θ2(t)) * l5 * m3 - sin(θ2(t)) * l5 * m4) * diff(diff(θ2(t), t), t) + (-sin(θ2(t) + θ3(t) + θ4(t)) * l7 * m4 / 0.2e1 - sin(θ2(t) + θ3(t)) * l6 * m3 / 0.2e1 - sin(θ2(t) + θ3(t)) * l6 * m4) * diff(diff(θ3(t), t), t) - m4 * l7 * diff(diff(θ4(t), t), t) * sin(θ2(t) + θ3(t) + θ4(t)) / 0.2e1 + (-l0 * m4 - m3 * cos(θ2(t) + θ3(t)) * l6 / 0.2e1 - cos(θ2(t) + θ3(t)) * l6 * m4 - cos(θ2(t) + θ3(t) + θ4(t)) * l7 * m4 / 0.2e1 - m2 * cos(θ2(t)) * l5 / 0.2e1 - m3 * l0 - m1 * l0 / 0.2e1 - m2 * l0 - m3 * cos(θ2(t)) * l5 - cos(θ2(t)) *

l5 * m4) * diff(θ1(t), t) ^ 2 + (-m3 * cos(θ2(t) + θ3(t)) * l6 / 0.2e1 - cos(θ2(t) + θ3(t)) * l6 * m4 - cos(θ2(t) + θ3(t) + θ4(t)) * l7 * m4 / 0.2e1 - m2 * cos(θ2(t)) * l5 / 0.2e1 - m3 * cos(θ2(t)) * l5 - cos(θ2(t)) * l5 * m4) * diff(θ2(t), t) ^ 2 + ((-cos(θ2(t) + θ3(t) + θ4(t)) * l7 * m4 - m3 * cos(θ2(t) + θ3(t)) * l6 - 0.2e1 * cos(θ2(t) + θ3(t)) * l6 * m4) * diff(θ3(t), t) - m4 * diff(θ4(t), t) * l7 * cos(θ2(t) + θ3(t) + θ4(t))) * diff(θ2(t), t) + (-m3 * cos(θ2(t) + θ3(t)) * l6 / 0.2e1 - cos(θ2(t) + θ3(t)) * l6 * m4 - cos(θ2(t) + θ3(t) + θ4(t)) * l7 * m4 / 0.2e1) * diff(θ3(t), t) ^ 2 - m4 * diff(θ4(t), t) * diff(θ3(t), t) * l7 * cos(θ2(t) + θ3(t) + θ4(t)) - m4 * diff(θ4(t), t) ^ 2 * l7 * cos(θ2(t) + θ3(t) + θ4(t)) / 0.2e1;

ISSN 0148-7191